Article

Eigenmode Wavefront Decoupling Algorithm for LC–DM Adaptive Optics Systems

Yukun Wang, Dayu Li * and Chengbin Jin

State Key Laboratory of Applied Optics, Changchun Institute of Optics, Fine Mechanics and Physics, Chinese Academy of Sciences, Changchun 130033, China

* Correspondence: lidayu@ciomp.ac.cn

Featured Application: Adaptive optics in large aperture telescopes for wide band imaging.

Abstract: To realize the decoupling control of the dual corrector of liquid crystal (LC)–deformable mirror (DM) adaptive optics (AO) systems and prevent the loss of correction ability induced by coupling aberrations, a wavefront decoupling method based on DM eigenmodes was proposed. The coupling relationship of two correctors was studied, and the distribution of aberrations corrected using the DM and LC was investigated. First, a DM eigenmode matrix was derived according to the DM influence function. Then, aberrations were decomposed according to the Strehl ratio, and the projection of the LC response matrix on the DM eigenmode matrix, that is, the coupling term, was derived. Before using the LC corrector, the coupling item was eliminated for the decoupling of the two correctors, and the decoupling effect was verified through simulations. Finally, a 2 m telescope LC–DM AO system was developed to validate the proposed method. The simulation and experimental results showed that the root mean square of the DM-corrected residual after 55 eigenmodes' correction was 0.09 μm. After decoupling correction, the resolution of the 700–1700 nm wide band improved from 1.1 to 1 times the diffraction limit, which is 1.2 times better than that obtained using the traditional Zernike mode correction.

Keywords: adaptive optics; eigenmodes; wavefront decoupling

1. Introduction

Adaptive optics (AO) technology is indispensable to solve atmospheric turbulence interference and restore the diffraction limit resolution of ground-based large-aperture telescopes [1–3], and is widely used in laser shaping, fundus imaging, laser communication, and other aberration correction fields [4–6]. Currently, most AO systems of large-aperture telescopes work in the infrared waveband [7] because the wavelength of visible light is shorter than that of infrared, the intensity of atmospheric turbulence is proportional to $\lambda^{-6/5}$ (λ is the wavelength), and atmospheric turbulence in the visible light band is strong (the atmosphere coherence length r0 is small). Although AO system imaging in the visible waveband can be achieved, the cost and complexity of the system will increase significantly. The deformable mirror (DM) is the core corrector of traditional AO systems. The number of drive units is proportional to (D/r0)2, where D is the telescope aperture. Therefore, imaging in the visible waveband requires a high density of DM actuators. However, the mechanical manufacturing process leads to the limitations of the DM. Obtaining the number of DM actuators of >200 is difficult. When this number exceeds 200, the cost and processing difficulty sharply increase, and an increase in spatial density leads to a decrease in the amplitude, thus making the DM unable to work for large-aperture telescopes of >2 m in the visible wavelength. Wavefront aberrations can be divided into low-order aberrations and high-order aberrations according to spatial frequency. Usually, the peak-to-valley (PV) values of low-order aberrations are larger, which we call large

amplitude, while the PV values of high-order aberrations are relatively small, so we call this small amplitude. To simultaneously compensate for the low-order large amplitude and high-order small amplitude aberrations, some researchers have proposed a woofer–tweeter dual DM AO system. The woofer was used to correct large amplitude, low spatial frequency aberrations and the tweeter was employed to correct small amplitude, high spatial frequency aberrations [8]. Currently, the DM with the most units worldwide is installed on the PALM-3000 system on the 5 m Haier Telescope in the United States. For this DM, the number of actuators is 3888, and the driving stroke is only 2 μm. It must be used in conjunction with a 241-actuator DM to obtain the image of Jupiter's Ganymede in the visible waveband. Due to its complicated coupling and control problems, no follow-up report on imaging in the visible waveband is available, and since 2010, the number of DM actuators has not increased [9,10].

Liquid crystal (LC) wavefront correctors present the advantages of high density, large amplitude, and low cost, which can compensate for the shortcomings of DMs. The principles and advantages of LC devices can be found in detail from reference [11]. However, due to the slow response of LCs in the long infrared waveband and severe LC dispersion in the broadened waveband, the working waveband of LCs is limited to 700–950 nm for a fast response without dispersion, which is narrower than that of DMs [12]. In 2016, researchers from the Changchun Institute of Optics, Fine Mechanics and Physics proposed a combination of a DM and LC as a wavefront corrector to completely exploit their advantages, overcome their shortcomings, and use the nondispersion feature of DMs to correct large amplitude low-order aberrations in the infrared and visible wavebands. LC is used to correct small amplitude high-order aberrations in the visible waveband, to meet the requirements of wide-band aberration correction [13,14]. Irrespective of whether a device is a dual DM system or an LC–DM system, the aberrations to be corrected are measured by a wavefront sensor (WFS). The distribution and decoupling methods of aberrations must be studied to prevent the correction loss caused by the opposite aberrations of each corrector, and the AO correction can be rendered unstable [15]. To achieve simultaneous working of dual correctors, researchers have proposed many decoupling control methods, including the two-step [16], Zernike limited term [17], control signal reset [18], Fourier mode [19], Lagrangian damped least square [20], and the wavelet mode decoupling [21] method. According to the results of reference [22], only two-step, Zernike limited term, and control signal reset methods are effective to suppress coupling aberrations. Other methods cannot make the system work stably for a long duration, due to the large amount of calculation and the accumulation of calculation errors. The two-step method is not suitable for dynamic correction. The Zernike limited items and control signal reset method can provide good results through closed-loop correction in the dual DM system. However, for LC–DM AO systems, LC works in the open loop to improve the energy utilization ratio [12]. The residual cannot be measured using a WFS, and the double DM decoupling method cannot be employed. A study used the Zernike mode to correct wavefront decomposition and proved the feasibility of LC–DM AO systems [13]. However, the fitting accuracy of the DM decreased with an increase in the number of Zernike modes [23]. Cross coupling is serious, and the correction effect must be improved.

In this paper, we proposed a wavefront decoupling method based on DM eigenmodes, which used the DM response matrix to construct the eigenmodes, thereby preventing the fitting error of the DM with the Zernike modes. Then, we discussed the wavefront decomposition method based on eigenmodes, and the aberrations in the infrared waveband were decomposed and corrected using the DM. The DM was controlled with eigenmodes to improve the compensation accuracy. The aberration in the visible waveband was compensated by the DM and LC. In order to ensure the aberration generated by LC does not include the aberration that has been corrected by the DM, the decoupling control method of LC and the DM must be studied. The reason for cross coupling between the two correctors was analyzed, and we calculated the projection of the LC response matrix on the DM eigenmode response matrix to obtain the coupling term of the two matrices when

correcting the same wavefront. Then, the control signal of LC was reset with the coupling term to realize aberration decoupling between the two correctors, thereby achieving high-precision correction in the visible waveband. Finally, a setup of the LC–DM AO system was developed for a 2 m telescope. The experimental results showed that the proposed method can effectively realize dual corrector decoupling. Compared with the correction accuracy of the traditional Zernike decomposition method, the correction accuracy of the proposed method was considerably improved.

2. Principle of the LC–DM AO System

2.1. System Composition

Figure 1 presents the block diagram of the LC–DM cascade AO system. This system is mainly composed of an LC wavefront corrector, a DM, a tip-tilt mirror (TTM), a Hartmann WFS, a wavefront processing computer, and an imaging camera. The density of the LC is 256 × 256 pixels, with a pixel size of 24 μm, and the aperture of the LC is 6.14 mm. The number of actuators of the DM is 145, the pitch of the DM is 2.5 mm, and its aperture is 30 mm. The aperture of the TTM is 25 mm and the number of subapertures of the WFS is 20 × 20, and the full aperture is 5.8 mm; these devices are placed in the conjugate position by lens pairs in the optical path for high spatial frequency small amplitude aberration correction, low spatial frequency large aberration correction, tilt aberration correction, and wavefront measurements, respectively. The wavefront processing computer is used for wavefront reconstruction, wavefront decoupling, and the calculation of the drive signal of each corrector. The wavefront obtained using the WFS is decomposed and decoupled and sent to the controller of each corrector. The controller is used to calculate the driving signal and to send this signal to each corrector. The imaging camera is employed to image the corrected light beam. In the design, the compactness and complexity of the system are comprehensively considered, and the device is selected by ensuring energy utilization, resolution, the field of view, and the zoom beam, and is completed with the smallest volume and fewest devices.
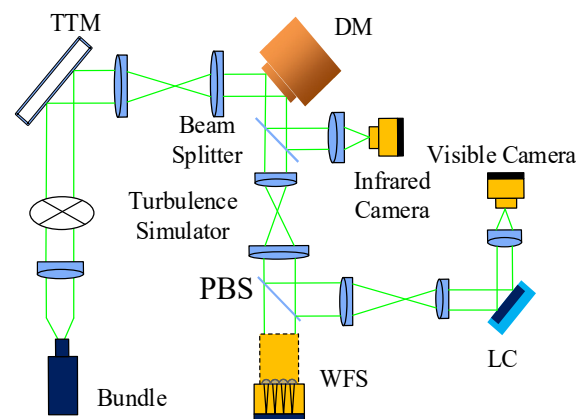
Figure 1. Block diagram of the LC–DM AO system.

2.2. Working Principle

The incident interfered beam obtained using a turbulence simulator is a broad spectrum beam of the 400–1700 nm waveband. The TTM and DM are situated at the front end of the optical path and are connected in series with the WFS to form the closed-loop control system. The LC is situated in the rear of the optical path and the WFS. The LC optical path works in the open-loop control system. First, the full wavelength incident beam passes through the TTM to correct the tilt aberration, and the DM is used to correct the low-order aberration to eliminate the wavefront aberration in the 950–1700 nm infrared waveband. The 950 nm beam is reflected through the beam splitter and enters the infrared imaging system. The transmitted beam is split by the 700 nm Polarized Beam Splitter (PBS), and after correction through the DM, the 400–700 nm band beam with the most comprehensive

aberration information enters the WFS for residual aberration measurements. The low-order distortion residuals and high-order distortion aberrations are decomposed to the DM and LC, respectively, in the front and rear optical paths, respectively. In addition, the short wavelength band of 700–950 nm enters the LC, and the remaining high-order aberrations are corrected according to the feed-forward signal of the WFS. Finally, diffraction-limited high-resolution imaging is obtained in a visible camera.

3. Materials and Methods

3.1. Construction of the DM Eigenmode Matrix

In most AO systems with dual (multi) DMs, the Zernike mode method is used to decompose wavefront aberrations. Then, DMs are used to produce the conjugated Zernike mode to correct distortion and aberrations. However, due to their parameters and other factors, DMs cannot achieve a perfect fit to the Zernike mode. The ith response function of the DM R_i was described as a Gaussian function in Formula (1). The LC was described by 209 Zernike modes, and the dimension of the wavefront is 256×256 pixels.

$$R_i = \exp\left[\ln \omega \left(\sqrt{(x - x_i)^2 + (y - y_i)^2}/d\right)^\alpha\right] \tag{1}$$

where α, ω, and d are the Gaussian exponent, the coupling value, and the spacing between the actuators in the DM, respectively. In this model, α was 1.73, ω was 0.23, and d was set to 0.083. These parameters are normalized values from the DM that was purchased from ALPAO. Figure 2 presents the residual aberration histogram of the top 54 Zernike modes with the 145 unit-DM, when the DM actuator stroke is not considered. Correction residual aberrations exhibit an overall upward trend with an increase in the number of modes mainly because when the number of modes increases, the spatial frequency of the wavefront is high, and the wavefront is considerably complicated. DMs cannot satisfy the requirements of high spatial resolution; the correction effect can be poor. Therefore, when the Zernike mode is used for wavefront decomposition and correction, fitting errors inevitably occur.
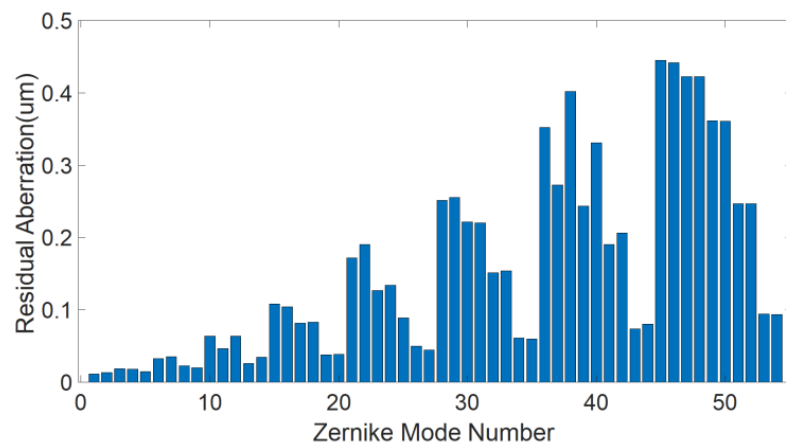

Figure 2. Fitting error of the top 54 Zernike modes with 145-unit *DM*.

Next, we give the derivation procedure of the DM eigenmodes. The response matrix, a two-dimensional matrix, is measured using the WFS. The response function of each actuator represents the response surface of each actuator. The final surface shape of the DM can be expressed through a linear combination of the response functions of each actuator:

$$\varphi = \sum_{i=1}^{n} v_i R_i \tag{2}$$

where n represents the number of actuators and v_i denotes the voltage applied using the *i*th actuator. The coupling relationship between the response functions can be expressed with a coupling matrix *C*, where the coupling values *C(i,j)* of the *i*th and *j*th actuators are calculated as follows:

$$C(i,j) = C(j,i) = D^{-1} \int_D R_i R_j dx dy \tag{3}$$

where *D* is the DM aperture. *C* describes the correlation of the influence functions of different actuators and may be decomposed using the singular value decomposition method:

$$C = USU^T \tag{4}$$

where *S* is the diagonal matrix whose diagonal elements are the eigenvalue of matrix *C*, *U* is the unitary matrix comprising the eigenvector of *C*, and *U* − 1 = *UT*. The linear combination of the response function of each actuator and the coupling matrix eigenvector constitutes a new two-dimensional matrix, the DM eigenmodes:

$$M_i = \sum_{j=1}^{n} U(i,j)R_j, i = 1, 2, \cdots, n \tag{5}$$

where M_i is the *i*th DM eigenmodes. As *U(i,:)* is the eigenvector of the *i*th actuator, the eigenvectors are orthogonal, so the eigenmodes are also orthogonal. There are n eigenmodes, which is the same as the number of actuators. A random wavefront may be described with the following eigenmodes:

$$\varphi = \sum_{i=1}^{n} m_i M_i \tag{6}$$

where m_i is the *i*th coefficient of M_i. Considering a 145-element DM from ALPAO in the laboratory as a prototype, Figure 3 shows the surface shapes of the top 27 eigenmodes.
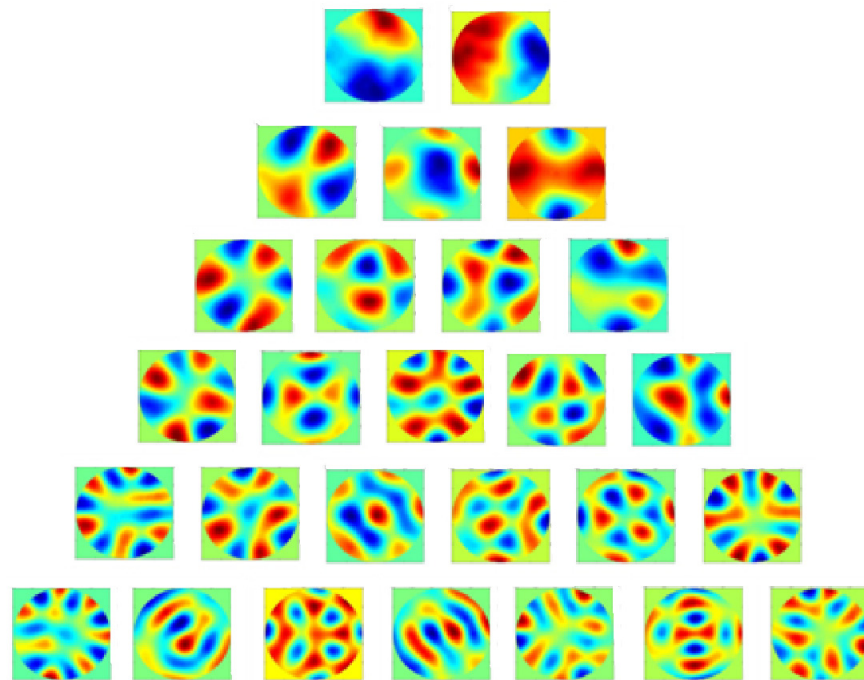

Figure 3. Top 27 eigenmodes' profiles of the 145-unit *DM*.

From the derivation procedure of the DM eigenmodes, it can be seen that the eigenmodes have the following properties: (1) The number of eigenmodes of a DM is equal to the number of its actuators. (2) The eigenmodes of the DM are orthogonal to each other.

(3) As the number of modes increases, the spatial frequency of the eigenmodes increases gradually. In addition, since the eigenmodes are obtained by constructing the response function of the DM, which reflects the inherent characteristics of the DM, there is no fitting error when using the DM to generate the eigenmodes. Compared with the Zernike modes presented in Figure 2, no fitting error is observed for eigenmodes in theory. Hence, the DM eigenmodes can effectively lead to a decrease in fitting errors and improvement of the final correction accuracy.

3.2. Eigenmode Correction Principle

After the eigenmodes are established, the wavefront can be reconstructed. This reconstruction process is similar to that of the Zernike mode. Because φ and Mi are two-dimensional matrices in Formula (6), for convenience of expression, the matrices φ and Mi are converted into columns $\overline{\varphi}$ and $\overline{M}_i$, respectively (the function of Matlab $\overline{\varphi}$ = reshape (φ, [], 1)), then Formula (7) can be expressed as follows:

$$\overline{\varphi} = M \cdot m \tag{7}$$

where $M = \left[\overline{M}_1, \overline{M}_2, \cdots, \overline{M}_n\right]$ is the DM eigenmode response matrix, and $m = [m_1, m_2, \cdots, m_n]^T$ is the eigenmode coefficients. The corresponding eigenmode coefficients of $\overline{\varphi}$ can be obtained using the least square method:

$$m = M^{-1} \cdot \overline{\varphi} \tag{8}$$

where $\overline{\varphi}$ is the measured distorted wavefront, and M^{-1} is the pseudo-inverse of the eigenmode matrix M. Moreover, the ith DM eigenmode and the DM voltage signal vector can also be obtained using the least square solution:

$$\overline{M}_i = \overline{R} \cdot v_{M_i} \Rightarrow v_{M_i} = \overline{R}^{-1} \cdot \overline{M}_i \tag{9}$$

where $\overline{R} = \left[\overline{R}_1, \overline{R}_2, \cdots, \overline{R}_n\right]$ $\overline{R}_i$ is the column vectors of the response matrix of each actuator, and v_{M_i} is the drive voltage vector corresponding to the ith eigenmode. Combining Formulas (7)–(9), the voltage vector v corresponding to the arbitrary wavefront $\overline{\varphi}$ expressed in the eigenmodes is obtained as follows:

$$v = v_M \cdot m = v_M \cdot M^{-1} \cdot \overline{\varphi} \tag{10}$$

where $v_M = \left[v_{M_1}, v_{M_2}, \cdots, v_{M_n}\right]$ is the driving voltage matrix corresponding to the eigenmode response matrix M. For Formula (10), v_M and M^{-1} can be obtained in advance. The voltage vector v is sent to the DM for wavefront correction. Figure 4 shows an original wavefront with the PV and RMS of 3.66 and 0.52 µm, respectively. After eigenmode correction, the PV and RMS decreased to 0.41 and 0.03µm, respectively.

(a)

(b)
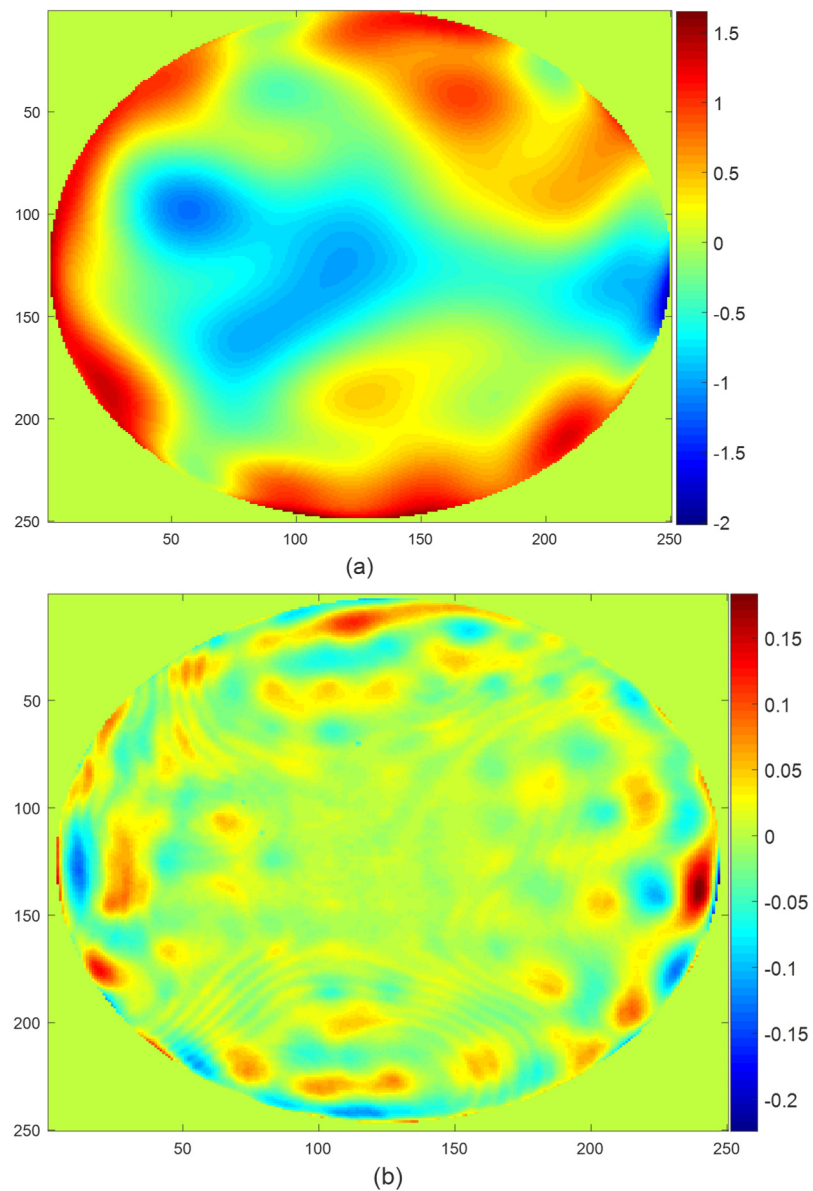
Figure 4. Simulation results of DM eigenmode correction (**a**) before and (**b**) after correction.

3.3. Decoupling of the LC–DM AO System

There are three steps in the decoupling procedure. The first step is wavefront decomposition. For the proposed LC–DM cascaded AO system, the DM is required to correct low-order large amplitude aberrations to meet the imaging requirements of the infrared waveband. To make the DM correct only the first N eigenmodes, the coefficient matrix m is selected as follows:

$$m' = I_N \cdot m \tag{11}$$

where I_N is an n $\times$ n identity matrix, the first N diagonal elements are 1, and the rest of the diagonal elements are 0, that is

$$I_N = \begin{bmatrix} 1 & & & & & & 0 \\ & \ddots & & & & & \\ & & 1 & & & & \\ & & & 0 & & & \\ & & & & \ddots & & \\ 0 & & & & & & 0 \end{bmatrix} \tag{12}$$

Substituting Formulas (11) and (12) into Formula (10), the control voltage vector v' can be used to calculate for the correction of the first N eigenmodes:

$$v' = v_M \cdot m' = v_M \cdot I_N \cdot M^{-1} \cdot \overline{\varphi} \tag{13}$$

After voltage calculation, the actual surface shape of the DM is obtained by employing the voltage and the DM response matrix. After the subtraction of the actual DM surface shape from the aberration to be corrected, the residual wave surface is sent to the LC:

$$\overline{\varphi}_{LC} = \overline{\varphi} - \overline{\varphi}_{DM} = \overline{\varphi} - \overline{R} \cdot v' \tag{14}$$

where $\overline{\varphi}_{LC}$ is the wave surface to be corrected, which is sent to the LC and $\overline{\varphi}_{DM}$ is the surface shape generated with the DM. Because the LC has thousands of pixels, if individual pixels are driven one by one, the calculation will be highly complicated and time-consuming; hence, the LC is driven with the Zernike mode surface. The wavefront correction process of the LC is as follows [12,13]

$$C = T^{-1} \cdot \overline{\varphi}_{LC} \tag{15}$$

where C and T are the control signal and response matrix of the LC, respectively. So far, we have obtained the wavefront that needs to be corrected by the LC. This part of the wavefront is the residual wavefront after the DM correction.

The second step is to obtain the coupling term between the LC corrector and the DM. In the LC–DM cascade AO system, the DM uses the eigenmode method for wavefront decomposition and reconstruction, which is different from the LC with the Zernike modes. The DM eigenmodes are obtained from the DM response, thus the DM can accurately fit its own eigenmodes without affecting the LC correction. The DM control voltage is calculated using Formula (13). For the LC corrector, the residual aberration is corrected using the Zernike modes. As there is no orthogonal relationship between the Zernike modes and the eigenmodes, the LC will generate the eigenmodes that have been corrected by the DM. That is to say, there are aberrations that have been corrected by the DM, which causes a reduction in the final correction performance. This part of the DM-corrected aberration $\overline{\varphi}_{coup}$ is the coupling term to be calculated and eliminated.

We first calculate the wavefront generated by the LC without decoupling. The control matrix C for the LC can be calculated using Formulas (13)–(15). The LC response wavefront can be expressed as follows:

$$\varphi_{LC\_response} = T \cdot C \tag{16}$$

There are aberrations that have been corrected by the DM in $\varphi_{LC\_response}$. To avoid the repetitive generation of the coupling aberration $\overline{\varphi}_{coup}$ by the LC, the DM eigenmodes M is used to reconstruct the LC wavefront $\varphi_{LC\_response}$

$$\varphi_{LC\_response} = M \cdot m_{LC} \tag{17}$$

where m_{LC} are the eigenmode coefficients corresponding to $\varphi_{LC\_response}$. Because the DM corrects the aberrations of the first N eigenmodes, the wavefront reconstructed with the LC should not contain the first N eigenmodes, thus the first N eigenmode coefficients of $\varphi_{LC\_response}$ is the coupling aberration that must be filtered out. Therefore, the coupling aberration can be calculated as follows:

$$\overline{\varphi}_{coup} = M \cdot I_N \cdot m_{LC} \tag{18}$$

So far, the coupling term is obtained with Formula (18), and the coefficient C_{coup} can be calculated with Formula (15). The third step is to subtract the coupling term to reset the control signal sent to the LC, thus the control signal sent to the LC after decoupling is as follows:

$$C' = C - C_{coup} \tag{19}$$

At this time, the coupling aberration is filtered out, and the aberration decoupling between the two correctors is realized. This is a type of control signal reset method. The basic principle is to remove the coupling term from the original signal.

3.4. Selection of the Eigenmode Number

In general, when the Strehl ratio (SR) reaches 0.8 in an optical system, high-contrast diffraction-limited resolution imaging can be achieved. According to this standard, the SR at the central wavelength of each imaging waveband should reach 0.8 after AO correction. The relationship between the SR and the wavefront residual σ is as follows:

$$SR = e^{-(k\sigma)^2} \tag{20}$$

$$\sigma = 0.075\lambda \tag{21}$$

For a telescope with an aperture of D = 2 m, and moderate turbulence of r0 = 10 cm at λ = 550 nm and r0 = 25.5 cm at λ = 1200 nm, when 55 eigenmodes are corrected, the wavefront residual is 0.073 λ. For the same parameters of D = 2 m and r0 = 19.3 cm at λ = 950 nm, 74 eigenmodes must be corrected to make this waveband reach the diffraction limit. In LC–DM cascade AO [13], the LC and DM are responsible for correcting 700–950 and 700–1700 nm wavebands, respectively. When the wavefront residual is <0.075 λ, both the bands can achieve diffraction limit resolution. According to the eigenmode number and wavefront residual formula presented in [24], the DM is used to correct only the top 55 eigenmodes to make the infrared waveband reach the diffraction limit, and the LC is employed for secondary correction on the residual wavefront after DM correction. After calculation, the LC must be used to correct the top 69 Zernike modes to attain 0.073 λ. Figure 5 presents the simulation of 50 wavefronts for a moderate intensity turbulence with a diameter D of 2 m and an r0 of 10 cm at λ = 550 nm. The proposed wavefront decoupling algorithm is used for simulation. According to the simulation results, the root mean square error (RMS) of residual aberration is approximately 0.09 μm after the correction of 55 eigenmodes, and 69 Zernike modes are used for residual aberration. After un-decoupling and decoupling correction, the residual errors are approximately 0.05 and 0.03 μm, respectively. After decoupling, the correction residual error decreases by approximately 0.02 μm. The decoupled wavefront can significantly improve the LC–DM correction accuracy.
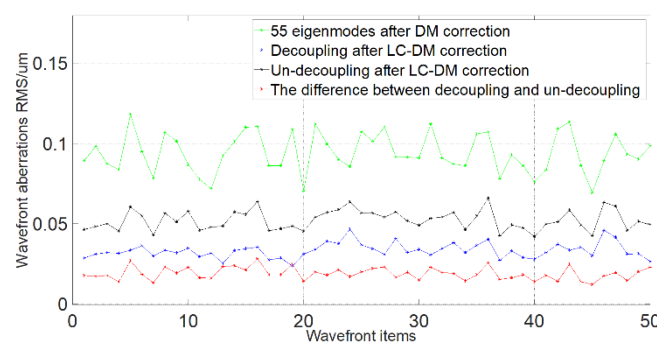

Figure 5. Curve of the wavefront correction RMS difference before and after decoupling.

4. Results

To verify the proposed decoupling algorithm, we developed an LC–DM AO system suitable for a 2 m aperture telescope in the laboratory. First, the DM was controlled using the eigenmodes. The aberration in the infrared band was corrected, and the results obtained with the Zernike mode were compared. Then the LC was controlled to compensate the residual aberration in the visible band and to compare the imaging effects of the decoupling and nondecoupling algorithms.

4.1. Experimental Setup

The setup of the LC–DM cascade AO system was constructed in the laboratory for a 2 m telescope (Figure 6). The system mainly constitutes two parts, namely AO and imaging parts. The AO part mainly includes the TTM, DM, LC, and the WFS. The DM is a 145-unit continuous surface DM produced by ALPAO, with an aperture and a stroke of 30 mm and approximately 3 μm, respectively. The LC is manufactured by Meadowlark optics Company, with the fast LC materials synthesized by us. The number of pixels is 256 × 256, the response time is 0.65 ms, and the effective aperture is 6.14 mm. The WFS is an SH wavefront sensor manufactured by FIRST-LIGHT company. The camera frame rate is approximately 1.67 kHz, the pixel size is 24 μm, and the number of microlenses is 20 × 20. The receiving aperture is approximately 5.8 mm. The imaging part includes visible and infrared cameras. The visible camera is an iXon ultra 897 model camera produced by ANDOR, with a pixel size of 16 μm, a number of pixels of 512 × 512, and a spectral response range of 400–900 nm. The infrared camera is a Cheetah-640CL short-wave infrared camera produced by the Xenics company, with a pixel size of 20 μm, a number of pixels of 320 × 256, and a spectral response range of 900–1700 nm.
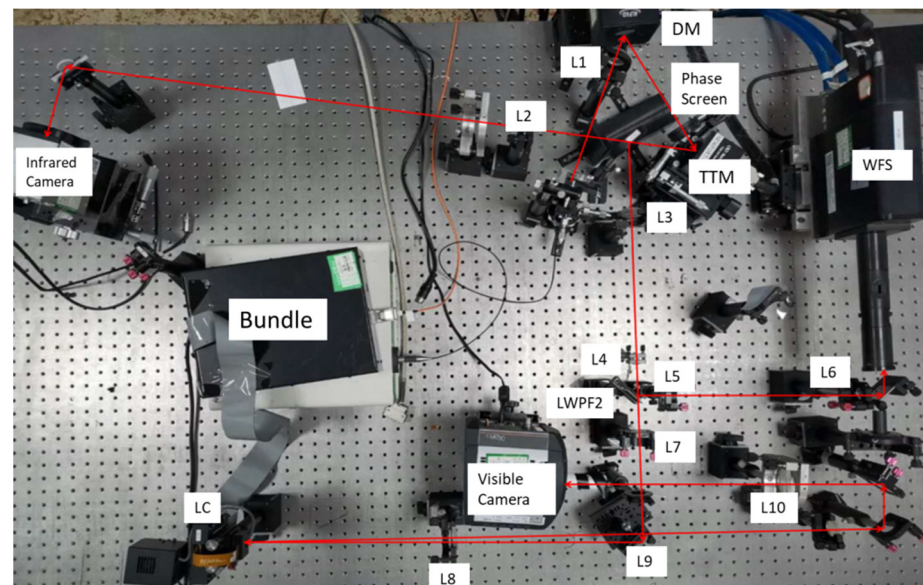
Figure 6. Optical layout of the LC–DM AO system.

For AO correction in a wide band range, in the system, a xenon lamp with a wavelength of 400–1700 nm is selected as the light source. After collimating through lens L1, the beam becomes parallel with a clear aperture of 20 mm. Producing chromatic aberration during collimation is easy. Hence, the KF51 + TF3 + KF51 triplet is used to achieve the purpose of an achromat. After the light beam is reflected through the DM and TTM, it is split using a 950 nm high-pass dichroic. The light with the 950–1700 nm waveband passes through the dichroic and is focused using the focusing lens L2 onto the infrared camera for imaging. For the reflected 400–950 nm waveband, L3 and L4 are contracted, and then, the beam is split using a 700 nm high-pass dichroic. The light of 700–950 nm passes through the dichroic, and the 400–700 nm beam is reflected. The beam is expanded using a 4f system composed of L5 and L6.

Subsequently, the beam is reflected through another 700 nm high-pass dichroic plate and enters the WFS for aberration measurements. The light with the 700–950 nm waveband that passes through the 700 nm high-pass dichroic plate is incident on the LC after being expanded through lenses L7 and L8, and the corrected beam passes through the 4f system composed of L8 and L9. After two reflections, this light is focused with focusing lens L10

onto the visible camera for imaging. Table 1 presents the parameters of each lens of the system.

Table 1. Parameters of each lens in the LC–DM adaptive optics system.

| Lens	Focus Length (mm)	Aperture (mm)
L1	200	20
L2	548	20
L3	300	20
L4	−43.5	2.9
L5	100	2.9
L6	200	5.8
L7	150	2.9
L8	300	5.8
L9	300	5.8
L10	272	5.8

In the system, the DM, LC, and WFS are all in the conjugate position. After the correction of the low-order aberrations of the whole band by using the DM, the infrared 950–1700 nm band can provide ideal imaging. Then, the residual error remaining after DM correction is passed to the LC for the secondary correction. At this time, low-order components in the residual error are eliminated, leaving only high-order aberrations in the 700–950 nm waveband. After the secondary correction through the LC, the AO correction and imaging of the 700–1700 nm wide band are realized.
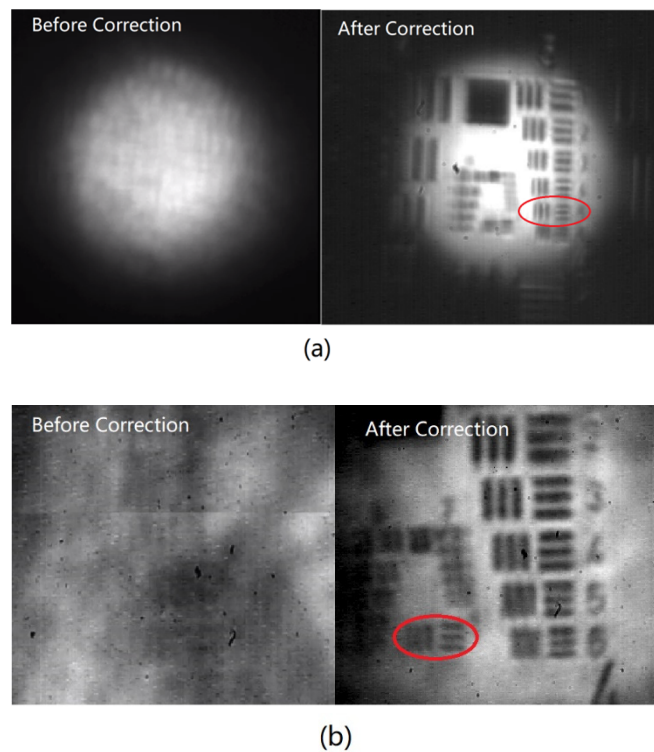
4.2. Results of Eigenmode Correction

First, the initial 55 eigenmodes were experimentally corrected according to Section 3.4. The turbulence simulator was placed at the system aperture diaphragm. The system aberrations detected through the WFS were PV = 4.32 μm and RMS = 0.71 μm (Figure 7). After the correction of the top 55 aberrations through the DM, the PV and RMS decreased to 1.21 and 0.08 μm, respectively. Figure 7b presents the wavefront of the residual aberration. According to the relationship between the residual RMS and the number of eigenmodes reported in [24], after the correction of 55 eigenmodes, the wavefront residual RMS can be lowered to approximately 0.47 rad, that is 0.07 μm, for the 950 nm waveband. Hence, the correction results are consistent with the theoretical results, and better than the finding of an RMS of 0.12 μm with the Zernike modes presented in [13].

After we obtain the wavefront aberration of the system, we can simulate the point spread function (PSF) of the system and calculate the optical transfer function (OTF) of the system by Fourier transform of the PSF, and then take the absolute value of the OTF, that is, the modulation transfer function (MTF) of the system. The MTF reflects the relationship between spatial resolution and signal intensity. Since the RMS of the wavefront residual aberration is 0.07 μm, which is better than $1/14 \lambda$ in the 0.95–1.7 μm waveband, the MTF curve will be close to the diffraction limit. In order to experimentally prove that the resolution can reach the diffraction limit, the CG-USAF-1951-0 standard resolution plate was used as the observation target, and the imaging experiment was performed. The USAF target was placed near the light source, and the image was captured with the infrared camera before and after AO correction. Figure 8a shows the USAF target captured using the infrared camera in the 1.5–1.7 μm waveband before and after the DM correction. Before the DM correction, the camera was blurred, and the image details could not be distinguished. After the DM correction of the top 55 eigenmodes, the fifth element of the fifth group in the USAF target was distinguished, and the corresponding element spatial frequency was 50.8 line pairs/mm, that is, the resolution was 19.7 μm. The diffraction limit resolution of an optical system can be calculated by $1.22 \frac{\lambda}{D} f$, where λ is the wavelength, D is the pupil diameter, and f is the effective focus length. In this AO system, the aperture of the entrance pupil was 20 mm, the effective focus length was 200 mm, and the diffrac-

tion limit at the central wavelength of 1.6 μm was 19.5 μm. Therefore, the image of the 1.5–1.7 μm waveband attained diffraction-limited resolution after the DM correction. Figure 8b shows the 950–1500 nm waveband before and after correction. After correction, the first element of the sixth group was resolved. The corresponding spatial frequency was 64 line pairs/mm, that is, the resolution was 15.6 μm. The diffraction-limited resolution of the central wavelength at 1.2 μm was 14.6 μm. Therefore, the image in the 950–1500 nm waveband achieved diffraction-limited resolution.
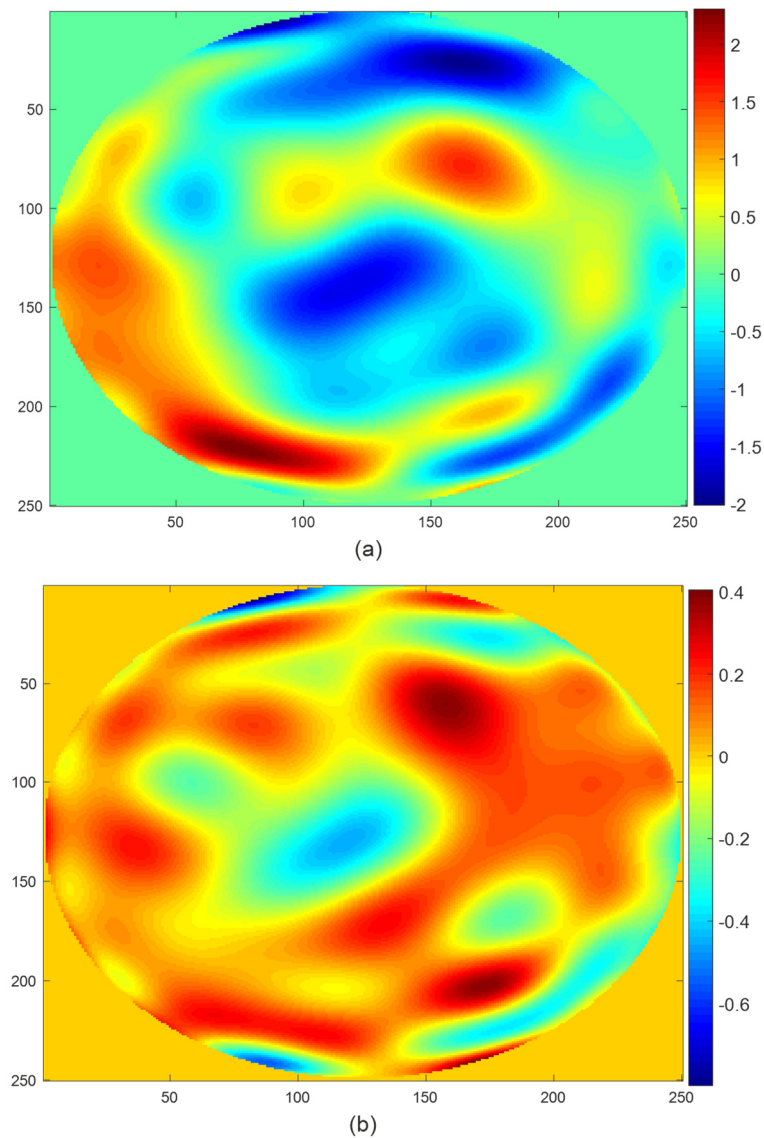
**Figure 7.** Wavefront detected with the WFS: (**a**) original and (**b**) residual wavefront after correction with the DM.

Figure 8. Infrared band resolution plate imaging: (**a**) 1.5–1.7 μm; (**b**) 950–1500 nm. (The clearest line pair has been circled in red).

4.3. Results of Decoupling Correction

After the elimination of the top 55 eigenmodes' aberrations with the DM, the 950–1700 nm waveband can achieve diffraction-limited imaging. The high-order aberrations are passed to the LC for secondary aberration correction in the 700–950 nm waveband, and the USAF target image is captured before and after correction. Because LC works in the open-loop working mode, the LC-corrected wavefronts cannot be detected with the WFS. Therefore, the wavefront before and after correction cannot be obtained; only the USAF target image can be obtained before and after correction from the visible camera.

Figure 9a shows the USAF target image obtained with the visible camera before the LC–DM correction. Due to the turbulence, the details of the USAF target image cannot be distinguished. Figure 9b presents the USAF target image obtained after the correction of the top 55 eigenmodes through the DM. Although the image resolution is improved, it cannot reach diffraction-limited resolution in the visible waveband. Figure 9c shows the USAF target image obtained after LC–DM correction without decoupling. The fourth element of the sixth group of the USAF target can be distinguished. The corresponding spatial frequency is 90.51 line pairs/mm, that is, the resolution is 11.04 μm. Figure 9d shows the image obtained after decoupling correction, with the corresponding spatial frequency of 101.6 line pairs/mm, that is, the resolution is 9.84 μm.
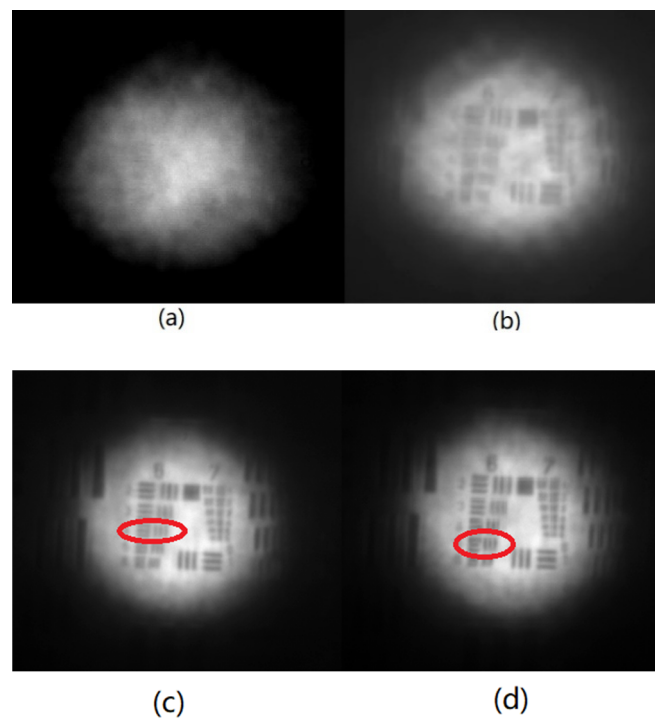
Figure 9. Image captured with the visible camera at 700–950 nm: (**a**) original image without correction; (**b**) image before correction using the *LC* and after correction through the *DM*; (**c**) image after nondecoupling correction with the *LC* and *DM*; (**d**) image after decoupling correction through the LC and DM. (The clearest line pair has been circled in red).

5. Discussion

From the experimental results, it was found that a DM can be used to correct 55 eigenmodes' aberrations, and 69 residual Zernike mode aberrations are compensated through the LC. Without decoupling correction, only the fourth element of the sixth group can be distinguished. After decoupling correction, the fifth element of the fifth group becomes visible, and the image achieves diffraction-limited resolution. The resolution is 1.2 times better than the result obtained using the Zernike mode decomposition method presented in [13], indicating that the proposed method can be effectively used to correct aberrations in the 700–1700-nm waveband and achieve diffraction-limited resolution. The proposed method can simultaneously control the LC and the DM, which is better than the two-step method used in [12] and can cope with turbulence with faster changing speed.

6. Conclusions

In this paper, a wavefront decoupling control algorithm based on DM eigenmodes is proposed for the LC–DM AO system. The DM eigenmodes and the eigenmodes' DM correction method were derived. An initial wavefront with a PV = 3.66 μm and an RMS = 0.52 μm was corrected through eigenmode correction. After the DM correction, the PV and RMS were minimized to 0.41 and 0.03 μm, respectively. For a 2 m telescope, the turbulence intensity was r0 = 10 cm at λ = 550 nm; for the DM and LC, the number of correction modes can be fixed to 55 eigenmodes and 69 Zernike modes, respectively. After decoupling correction, the RMS of the residual aberration decreased by 0.02 μm. Finally, a setup of an LC–DM cascade AO system was developed, with a standard resolution plate as the imaging object. The imaging resolution in the 1.5–1.7 and 0.95–1.5 μm wavebands was 19.7 and 15.6 μm, respectively. These results indicated that the resolution reaches the diffraction-limited resolution in the infrared waveband. The imaging resolution without and with decoupling in the visible waveband of 0.7–0.95 μm was 11.04 and 9.84 μm, respectively, which is approximately 1.1 and 1 times, respectively, the diffraction-limited resolution. Therefore, the decoupling algorithm can achieve the diffraction-limited resolu-

tion in the visible waveband, which is 1.2 times better than the diffraction-limited resolution of the traditional Zernike mode algorithm. This algorithm can be used to expand the work waveband of AO systems in large aperture telescopes by approximately 250 nm at a low cost.

The proposed method can realize the cooperative control of two correctors and establish a foundation for the engineering applications of LC–DM cascade AO systems.

Author Contributions: This work was conducted by Y.W., D.L. and C.J. The conceptualization, methodology, and validation were conducted by Y.W. and D.L. conducted the software and formal analysis. C.J. completed the investigation, data curation, and original draft preparation. Y.W. was responsible for project administration and funding acquisition. All authors have read and agreed to the published version of the manuscript.

Institutional Review Board Statement: Not applicable.

Informed Consent Statement: Not applicable.

Data Availability Statement: The data presented in this study are available on request from the corresponding author.

Conflicts of Interest: The authors declare no conflict of interest.

References

1. Tyson, R.K.; Frazier, B.W. *Principles of Adaptive Optics*, 5th ed.; CRC Press: Boca Raton, FL, USA, 2022. [CrossRef]
2. Wang, Y.K.; Hu, L.F.; Wang, C.C. Modeling and control of Tip/Tilt Mirror in liquid crystal adaptive optical system. *Opt. Precis. Eng.* **2016**, *24*, 771–779. [CrossRef]
3. Wang, Y.; Hu, L.F.; Wang, C.C.; Wang, S.X.; Xuan, L. Adaptive inverse control for tip/tilt mirror in adaptive optical system. *Opt. Precis. Eng.* **2015**, *23*, 2203–2210. [CrossRef]
4. Qin, Z.; He, S.; Yang, C.; Yung, J.S.-Y.; Chen, C.; Leung, C.K.-S.; Liu, K.; Qu, J.Y. Adaptive optics two-photon microscopy enables near-diffraction-limited and functional retinal imaging in vivo. *Light. Sci. Appl.* **2020**, *9*, 79. [CrossRef]
5. Salter, P.S.; Booth, M.J. Adaptive optics in laser processing. *Light Sci. Appl.* **2019**, *8*, 110. [CrossRef] [PubMed]
6. Wang, Y.; Xu, H.; Li, D.; Wang, R.; Jin, C.; Yin, X.; Gao, S.; Mu, Q.; Xuan, L.; Cao, Z. Performance analysis of an adaptive optics system for free space optics communication through atmospheric turbulence. *Sci. Rep.* **2018**, *8*, 1124. [CrossRef] [PubMed]
7. Takami, H.; Colley, S.; Dinkins, M.; Eldred, M.; Guyon, O.; Golota, T.; Hattori, M.; Hayano, Y.; Ito, M.; Iye, M.; et al. Status of Subaru laser guide star AO system. *Proc. SPIE* **2006**, *6272*, 62720C.
8. Zou, W.; Qi, X.; Burns, S.A. Woofer-tweeter adaptive optics scanning laser ophthalmoscopic imaging based on Lagrange-multiplier damped least-squares algorithm. *Biomed. Opt. Express* **2011**, *2*, 1986–2004. [CrossRef] [PubMed]
9. Roberts, J.; Bouchez, A.H.; Burruss, R.S.; Dekany, R.G.; Guiwits, S.R.; Troy, M. Optical characterization of the PALM-3000 3388-actuator DM. *Proc. SPIE* **2010**, *77362*, 77362E.
10. Dong, Y.; Yao, K. Three hundred and fourty-nine unit adaptive optical wavefront processor. *Opt. Precis. Eng.* **2018**, *26*, 1007–1013.
11. Yin, K.; Hsiang, E.L.; Zou, J.; Li, Y.; Yang, Z.; Yang, Q.; Lai, P.C.; Lin, C.L.; Wu, S.T. Advanced liquid crystal devices for augmented reality and virtual reality displays: Principles and applications. *Light Sci. Appl.* **2022**, *11*, 161. [CrossRef]
12. Zhaoliang, C.; Quanquan, M.; Huanyu, X.; Peiguang, Z.; Lishuang, Y.; Li, X. Open loop liquid crystal adaptive optics systems: Progresses and results. *Proc. SPIE* **2015**, *9676*, 1–7.
13. Sun, F.; Cao, Z.; Wang, Y.; Zhang, C.; Zhang, X.; Liu, Y.; Mu, Q.; Xuan, L. DM/LCWFC based adaptive optics system for large aperture telescopes imaging from visible to infrared waveband. *Opt. Express* **2016**, *24*, 276491. [CrossRef] [PubMed]
14. Adamow, A.; Szukalski, A.; Sznitko, L.; Persano, L.; Pisignano, D.; Camposeo, A.; Mysliwiec, J. Electrically controlled white laser emission through liquid crystal/polymer multiphases. *Light Sci. Appl.* **2020**, *9*, 19. [CrossRef] [PubMed]
15. Yukun, W.; Zhaoliang, C.; Dayu, L.; Xu, H.; Li, X. Research on the design of Liquid Crystal-DM Adaptive Optical System Data Acquisition and Process Software. *Opt. Precis. Eng.* **2018**, *26*, 1507–1516.
16. Cense, B.; Koperda, E.; Brown, J.M.; Kocaoglu, O.P.; Gao, W.; Jonnal, R.S.; Miller, D.T. Volµmetric retinal imaging with ultrahigh-resolution spectral-domain optical coherence tomography and adaptive optics using two broadband light sources. *Opt. Express* **2009**, *17*, 4095–4111. [CrossRef]
17. Liu, W.; Dong, L.; Yang, P.; Lei, X.; Yan, H.; Xu, B. A Zernike mode decomposition decoupling control algorithm for dual deformable mirrors adaptive optics system. *Opt. Express* **2013**, *21*, 23885–23895. [CrossRef] [PubMed]
18. Cheng, T.; Liu, W.; Pang, B.; Yang, P.; Xu, B. A slope-based decoupling algorithm to simultaneously control dual deformable mirrors in a woofer–tweeter adaptive optics system. *Chin. Phys. B* **2018**, *27*, 070704. [CrossRef]

19. Jean-François, L.; Jean-Pierre, V. Woofer-tweeter control in an adaptive optics system using a Fourier reconstructor. *J. Opt. Soc. Am. A* **2008**, *25*, 2271–2279.
20. Zou, W.; Burns, S.A. Testing of Lagrange multiplier damped least-squares control algorithm for woofer-tweeter adaptive optics. *Appl. Opt.* **2012**, *51*, 1198–1208. [CrossRef] [PubMed]
21. Hampton, P.J.; Agathoklis, P.; Conan, R.; Bradley, C. Closed-loop control of a woofer–tweeter adaptive optics system using wavelet-based phase reconstruction. *J. Opt. Soc. Am. A* **2010**, *27*, A145–A156. [CrossRef] [PubMed]
22. Cheng, T.; Xu, Z.X.; Yang, K.; Wang, S.; Xu, B. A decoupling control algorithm for Woofer–Tweeter adaptive optics system in generalized irregular pupil region. *Opt. Commun.* **2020**, *472*, 125856. [CrossRef]
23. Hu, S.; Chen, S.; Xu, B.; Yang, P.; Cai, D.; Wu, J.; Jiang, W. Experiment of Double DMs Adaptive Optics System for Phase Compensation. *Proc. SPIE* **2007**, *6467*, 64670K.
24. Jin, C.; Zhang, X.; Sun, W.; Li, N.; Xuan, L. Correction performance estimation of atmospheric turbulence based on eigenmode method. *Opt. Commun.* **2020**, *466*, 125661. [CrossRef]